The 6th International Supercritical CO_2 Power Cycles Symposium
March 27 - 29, 2018, Pittsburgh, Pennsylvania

Advanced Gas Foil Bearing Design for Supercritical CO_2 Power Cycles

Peter A. Chapman, Jr., P.E.
Principal Engineer
Mechanical Solutions, Inc.
Albany, NY USA

Mr. Chapman is a Principal Engineer at Mechanical Solutions, Inc. in Albany, NY. He has been involved with development, testing, and evaluation of machinery systems throughout his career. At Mechanical Technology Incorporated (MTI) he held various engineering positions involved in development of Stirling engines and related mechanical systems. In 1998 Mr. Chapman joined Foster-Miller Inc. (now Qinetiq North America), to whom the MTI foil bearing business was sold, and where he was the principal designer of foil bearings and magnetic bearings for a variety of rotating machines ranging from miniature blood pumps and micro gas turbines to energy storage flywheels and high speed blowers. Mr. Chapman joined MSI following MSI's 2009 acquisition of the foil bearing business from FMI. He received his BSME Cum Laude from Union College and a Licensed Professional Engineer in the State of New York.

ABSTRACT

Because of its potential for high efficiency power generation, supercritical carbon dioxide (sCO_2) is receiving much attention as a potential power cycle working fluid. The sCO_2 power cycle gains a sizable advantage over conventional power cycles as turbine inlet temperatures and pressures increase. Traditionally lubricated and cooled oil bearings cannot tolerate the higher temperatures, and the higher pressures makes keeping the oil separate from the working fluid an increasingly difficult challenge. These conditions strongly promote the use of the sCO_2 working fluid itself as the lubricant, rather than oil.

To address this challenge, Mechanical Solutions, Inc. (MSI) is developing a new gas foil bearing that meets these advanced needs by using the sCO_2 as the lubricating fluid. The new bearing is also designed to overcome the traditional drawbacks of conventional foil bearings, such as low load capacity, and only modest stiffness and damping. The proposed concept combines the best features of hydrodynamic bearing technology with specific design enhancements of hydrostatic bearing technology that provide increased load capacity, stiffness, damping, wear resistance, and tolerance to severe service conditions, with greatly reduced and acceptable leakage allowance for the pressurized hydrostatic bearing cavities relative to conventional stand-alone hydrostatic bearing designs. The progress of this development program, including some of the analytical challenges inherent with the bearing design, is presented.

INTRODUCTION

Due to its ability to generate more efficient power over traditional supercritical- or superheated-steam cycles, supercritical CO_2 (sCO_2) power generation is getting significant consideration for new commercial applications. Because the sCO_2 power cycle gains much of its advantage through implementing higher turbine inlet pressures (up to 300 bar) and temperatures (up to 800°C), the need to improve power cycle machinery on the component level becomes essential. The combination of high pressure and temperature required for these systems poses a unique challenge to the design of the turbomachinery and their components. Particularly critical are the bearings of these systems. Bearings that are traditionally lubricated and cooled with oil, even with the best synthetic oils currently available on the market, cannot tolerate these extreme temperatures. Seal designs become extremely complex in order to contain the working fluid under the higher pressures, and maintaining separation of the oil and working fluid is increasingly difficult. This severe environment obviates the practicality of an oil system, encouraging the use of the working fluid as the lubricant. By eliminating the lube-oil system, an opportunity to design a hermetically sealed system arises, thereby eliminating the need for complex seal designs and permitting the sole use of internal labyrinth or brush seals. Elimination of the ancillary equipment (oil pumps, coolers, oil de-aerators, etc.) has the added benefit of reducing cost, complexity, and reliability issues inherent with an oil-lubrication system.

The author's company, Mechanical Solutions, Inc. (MSI), through a Small Business Innovative Research (SBIR) grant funded by the Department of Energy (DOE) Office of Fossil Energy, is developing a new gas foil bearing that meets these advanced needs by using the sCO_2 as the lubricating fluid. The goal of this project is to develop a reliable, high performance foil bearing system for supercritical CO_2 power cycle machinery. The bearing system will be capable of temperatures up to 800°C and pressures up to 300 bar. Key elements of the design include:

- An advanced hydrostatically-assisted hydrodynamic (or hybrid) foil bearing concept capable of much higher specific loads and stiffness than traditional hydrodynamic-only bearing designs.
- An integral gas delivery system that incorporates flow passages and geometric enhancements to distribute and control the flow throughout the bearing for the hydrostatic assist while reducing the total mass flow rate.
- The addition of overload protection designed to handle large shaft excursions in the event of system severe transients.
- An optimized foil arrangement that increases bearing hydrodynamic stiffness and damping, and provides additional load carrying capacity.
- The use of new high temperature materials and coatings that prolong the life of foil bearings, enabling sufficient start/stop cycles.

The author's development group has combined best-in-class technologies in pressurized hydrostatic gas bearings and hydrodynamic gas foil bearings to produce an advanced hybrid bearing system that can operate under these conditions without oil lubrication, providing the enabling technology needed to meet the challenges of advanced sCO_2 power cycles.

Based on the work accomplished and results obtained from the author's previous work[1], it was previously concluded that:

- A significant improvement in load capacity and stiffness can be gained over the traditional performance of a purely hydrodynamic gas foil bearing by including a hydrostatic assist component.

- The nature of the sCO_2 fluid is highly complex, requiring the development of a sophisticated analytical model to adequately simulate its behavior under the assumed conditions.
- Rotordynamically stable operation of the hydrostatic bearing is greatly enhanced in sCO_2 vs. air due to the much lower flow velocities in the bearing.
- A high temperature coating has been demonstrated to survive up to temperatures of 650°C with minimal wear over 1000 start/stop cycles, more than ample for the lifetime of a typical power cycle machine.

The above findings served as the starting point for the effort presented in the current paper.

RESULTS AND DISCUSSION

As presently envisioned, the bearing system will include separate radial bearings and thrust bearings. Depending on the specific machine configuration, one radial and one thrust bearing can be combined into a single-housed "combination" bearing to save space.

Journal Bearing Design

The advanced foil journal bearing is comprised of a top foil, a multi-layered bump foil, and bearing shell, as illustrated in Figure 1.

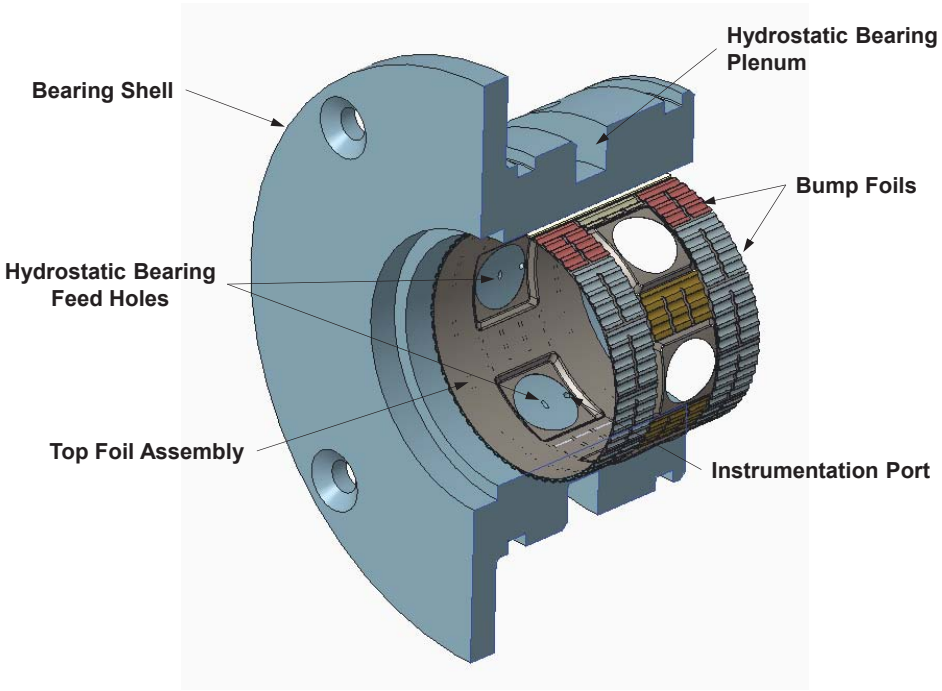

Figure 1: Advanced Foil Journal Bearing Construction

The top foil is traditionally a single smooth foil rolled into the circular shape of the bearing. To include the hydrostatic component to the bearing, an array of pockets is formed into the surface (see Figure 2). The working fluid (in this case sCO_2) is supplied to each pocket through an orifice that is drilled radially through the bearing shell. The pocket perimeter is laser welded around the orifice to eliminate bypass leakage around the bearing.

The introduction of the discrete pocket design came about from the Phase I work. Computational fluid dynamic (CFD) analysis of a simple orifice design shown in Figure 3, as studied and experimentally validated by Texas A&M University (Park[2] and Kumar[3]), revealed that a significant amount of pressure is not created in a large enough area around the hole, resulting in a low hydrostatic force. By adding the pocket surrounding the orifice, a larger pressure area can be created, resulting in a significantly larger hydrostatic force.

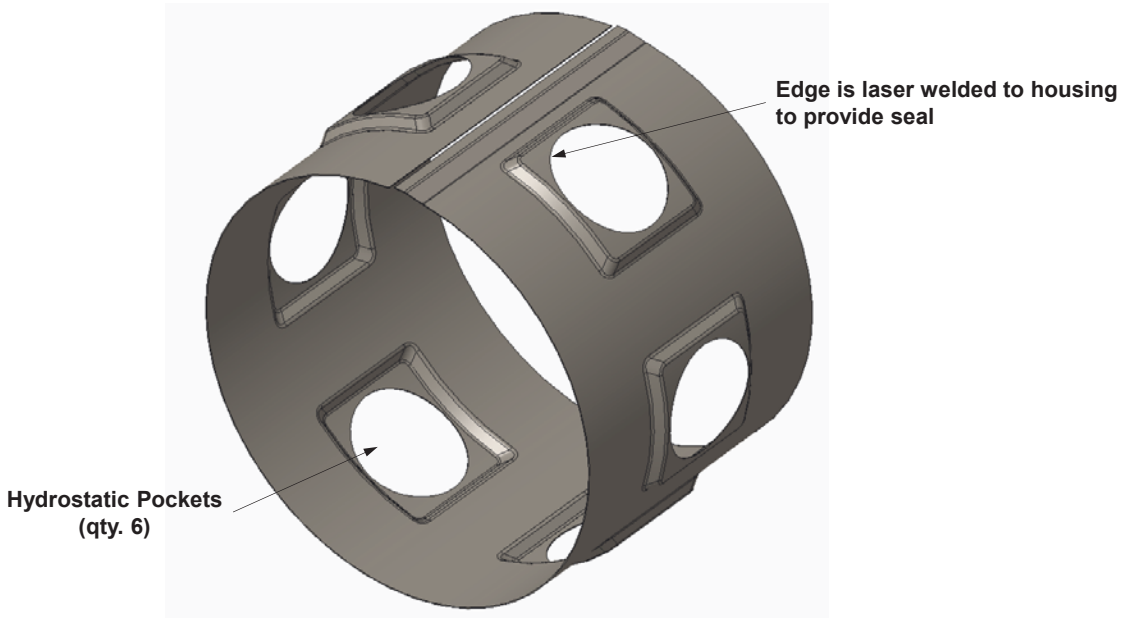

Figure 2: Hydrostatic Bearing Supply Details - Phase I Proposed Design

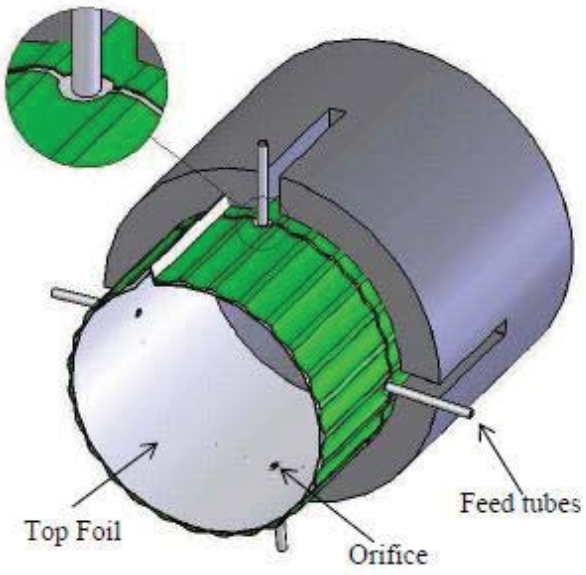

Figure 3: Schematic of a Hybrid Air Foil Bearing (HAFB) (courtesy Texas A&M University[1,2])

Underneath the top foil are two layers of bump foils stacked concentrically on top of each other (Figure 4). The bump foils are split circumferentially as traditionally done, providing axial compliance. The top bump layer, adjacent to the top foil, is a thinner, more compliant foil. This layer provides beneficial compliance to the foil bearing, allowing the bearing to deform to the pressure profile, limiting cross-coupling forces and thereby enhancing rotordynamic stability. The bottom bump layer, adjacent to the bearing shell, is thicker and therefore much stiffer than the top layer. This foil is spaced with a very small gap, on the order of 0.001 inch, between it and the top bump foil. As the load on the bearing increases, the top bump foil deflects until it contacts the bottom bump foil. This bottom foil provides added overload protection, as stiffness and load capacity increase dramatically, by a factor of five or more, but only on an as-needed basis.

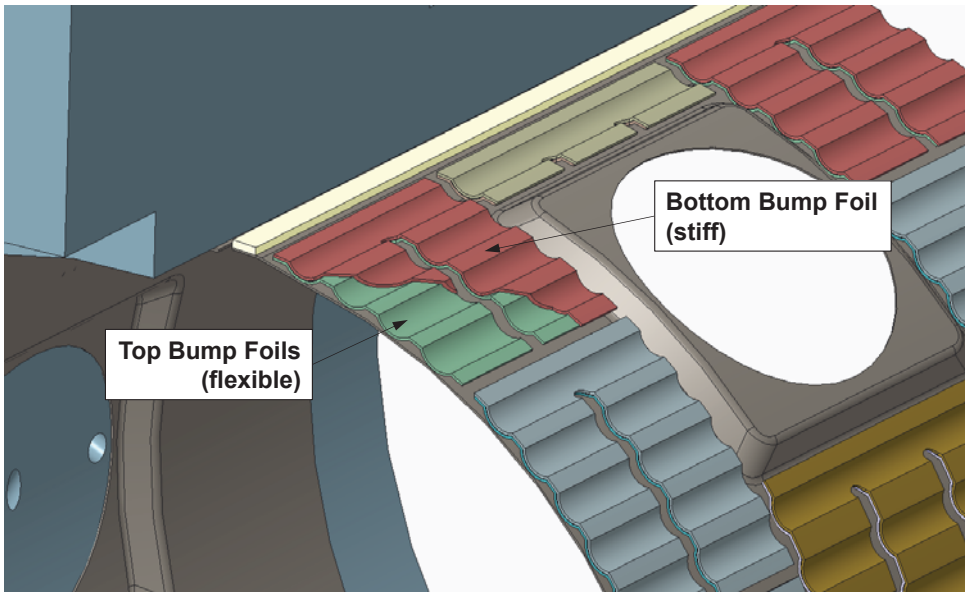

Figure 4: Bump Foil Arrangement Showing Different Foil Layers (Bottom bump foil is shown cut away for clarity)

Thrust Bearing

The thrust bearing is similar in construction to the journal bearing, as shown in Figure 5. It is comprised of multiple individual bearing pads, equally spaced around the circumference, mounted to a thrust plate. The pads are comprised of two layers of bump foils and a top foil, similar to the journal bearing. Each pad contains its own hydrostatic bearing feed passages, and each bearing is pressurized independently through the back thrust plate. Unlike the hydrostatic journal bearing, which has pressure feeds around the full circumference that tend to counteract each other, the hydrostatic pressure pockets in the thrust bearing all face the same direction and thus sum together. Therefore, the hydrostatic pockets are capable of generating a significantly higher net force with the same pocket geometry. This also has the benefit of being less sensitive to pressure and flow variations from one nozzle to the next since a force balance is not required. As such, the nozzles can be fed in parallel or series with minimal consequence to performance.

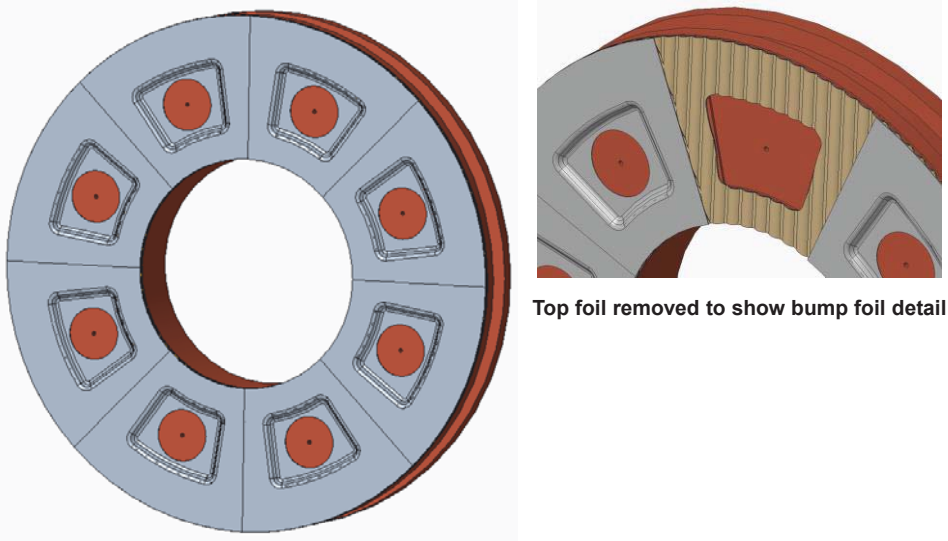

Figure 5: Advanced Foil Thrust Bearing Construction

Analytical Approach

To properly analyze the performance of the bearings, a series of computational models were developed. Performance characteristics that were sought out of the models included load capacity, direct stiffness (i.e. force generated in the direction of shaft motion), cross-coupling stiffness (i.e. force generated perpendicular to shaft motion), and damping coefficients (both direct and cross-coupling). The following steps were carried out in developing the modeling approach:

- Characterize the fluid properties of supercritical CO_2 for temperatures and pressures within the anticipated bearing operating range, with particular focus around the critical point.
- Evaluate performance optimization of the hydrostatic bearing, investigating several promising design variations
- Superimpose the hydrodynamic effect on the model, including synergistic effects
- Add the compliant foil sub-structure interaction to the model

Supercritical Fluid Properties Evaluation

Through the use of non-project funding, MSI has acquired detailed real gas properties (RGP) tables for CO_2 over a pressure range of 2 to 50 MPa and a temperature range of 200 K (-53°C) to 1500 K (1227°C), as illustrated in Figure 6. The tables support liquid, vapor, and supercritical states, include saturation curve data, and metastable states near saturation for both superheated liquid and subcooled vapor. Metastable states occur when the vapor cools below the local saturation temperature due to rapid flow expansion (a likely event at a hydrostatic bearing nozzle exit) or when the liquid temperature rises above saturation due to rapid heating or compression. The tables are suitable for single phase and binary mixture analysis within the ANSYS CFX solver.

In addition to their generation, the tables were then verified in three ways. First, the tables were cross-plotted against the charts produced directly from REFPROP. Next, the tables were

checked by solving a duct flow analysis over a wide range of different pressure and temperature levels to explore the full RGP table source. Finally, validation was conducted on the bearing geometry generated in Phase I and compared to the original results. Convergence problems originally experienced during Phase I were resolved by using an "expert parameter" (not available to typical public users of CFX), yielding steady-state convergence as well as an improvement in solution time on the order of 100 to one.

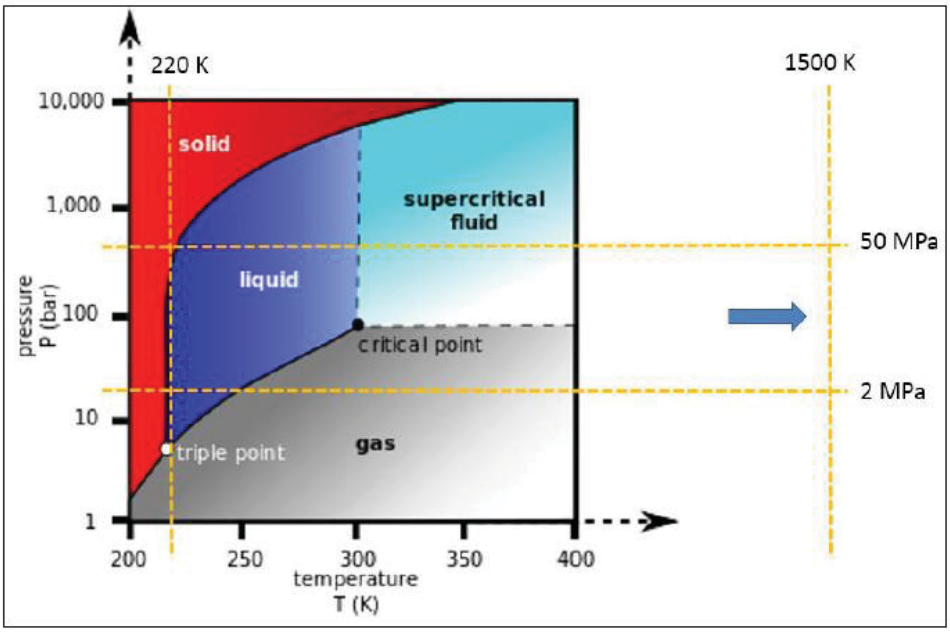

Figure 6: Diagram Showing Pressure and Temperature Ranges of the RGP Table

Computational Fluid Dynamic and Structural Analysis Studies

In an effort to characterize the performance of a foil bearing employing sCO_2, a series of CFD and structural finite element studies were completed. The primary intention of these studies was to understand the flow characteristics within the foil bearing, and the variables that control them, in order to develop a model that can be used to predict bearing performance. This study has gone through four primary steps:

1. The hydrostatic nozzle and pocket geometries were optimized using simplified geometry using a planar surface model.
2. A three-dimensional model of the full bearing geometry was created to predict the flows and pressures within the bearing.
3. The generated pressures were used as input into the structural model to determine foil stresses and deflections.
4. The CFD and structural models were iterated to obtain a converged solution of the pressures and deflections.

The results of the CFD studies are presented herein.

Geometry Optimization – Nozzle & Pocket Sizing

A CFD sector model was created to evaluate the effect the nozzle diameter, pocket size, pocket depth, and the addition of a diffuser has on a hydrostatic bearing application utilizing

sCO_2. The CAD model was parametrized so that dimensions could be changed and the mesh automated to study several configurations. Two models were created, a 90 degree sector and a 20 degree sector. The 90 degree sector (Figure 7) was used to evaluate the effectiveness of adding an obstruction of equal diameter to the nozzle in order to reduce the jet impingement effect on the shaft. The 20 degree sector (Figure 8) allowed for a relatively low solver time so that multiple configurations could be evaluated quickly. The final design configuration was modeled using a 180 degree, multi-nozzle configuration with an offset shaft to derive the true restoring force in the hydrostatic bearing, as discussed later.

The goal of this study was to come up with an optimum nozzle/pocket configuration that maximizes static pressure in the pocket (thereby maximizing the force) while minimizing the flow rate. In the system application, the flow for the hydrostatic bearings will be routed from the pump/compressor, so limiting the flow rate will benefit the overall system efficiency. Typical contour plots comparing the velocity and pressure distributions in a diffuser with and without an obstruction are shown in Figure 9 and Figure 10 respectively. The analysis showed that the presence of the obstruction increased the load force only a small amount (less than 4 percent) while increasing mass flow rate by 25 percent. Based on this, the obstruction approach was abandoned.

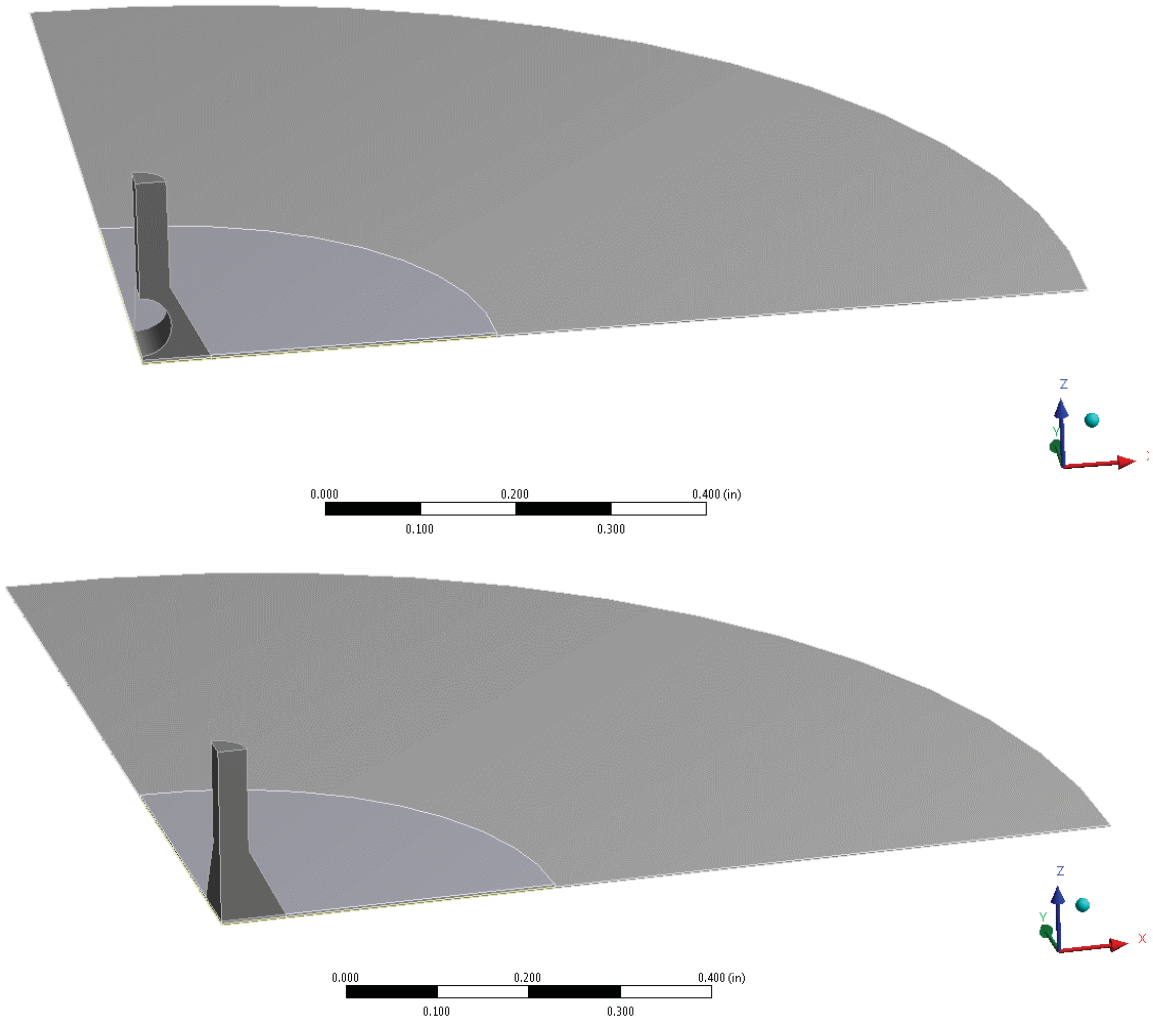

Figure 7: 90 Degree Sector Model used for Evaluating an Obstruction at the Nozzle Entry

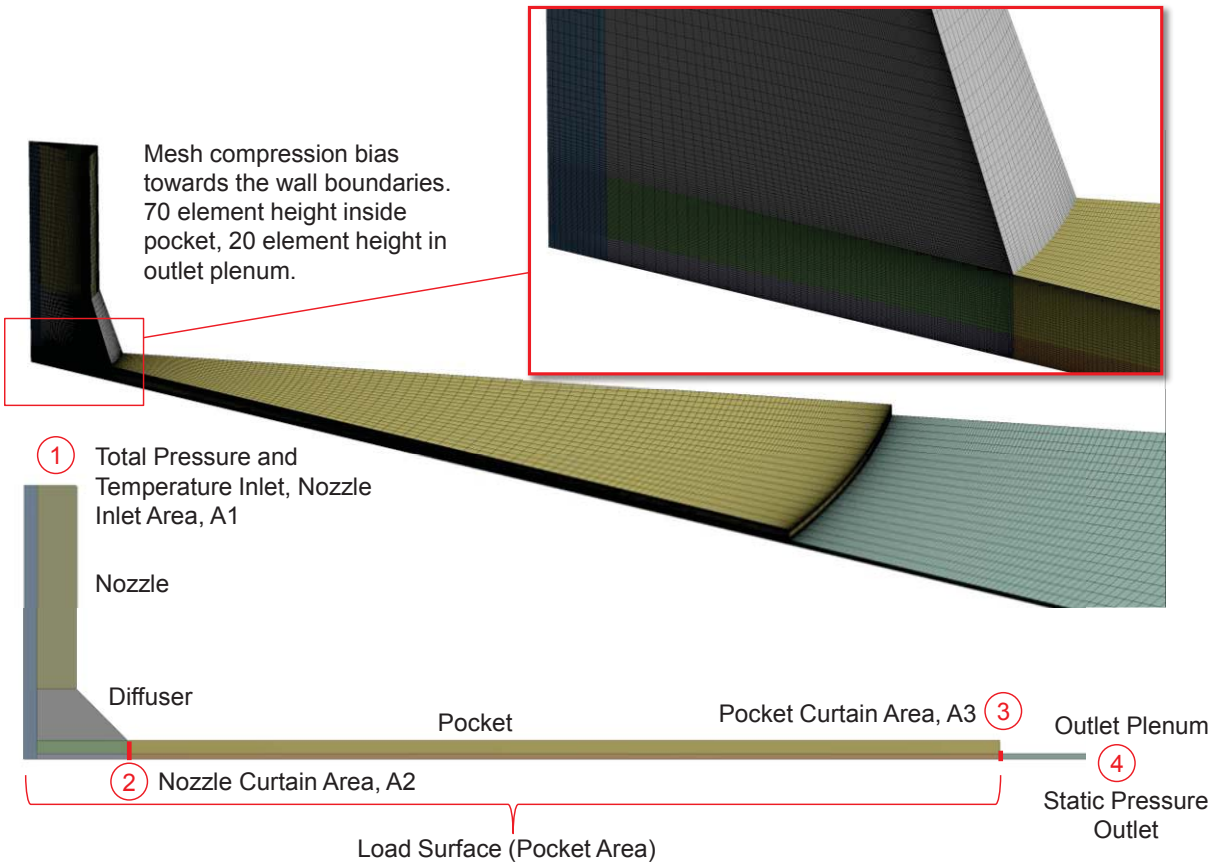

Figure 8: 20 Degree Sector Model used for Fast Evaluation of Different Configurations

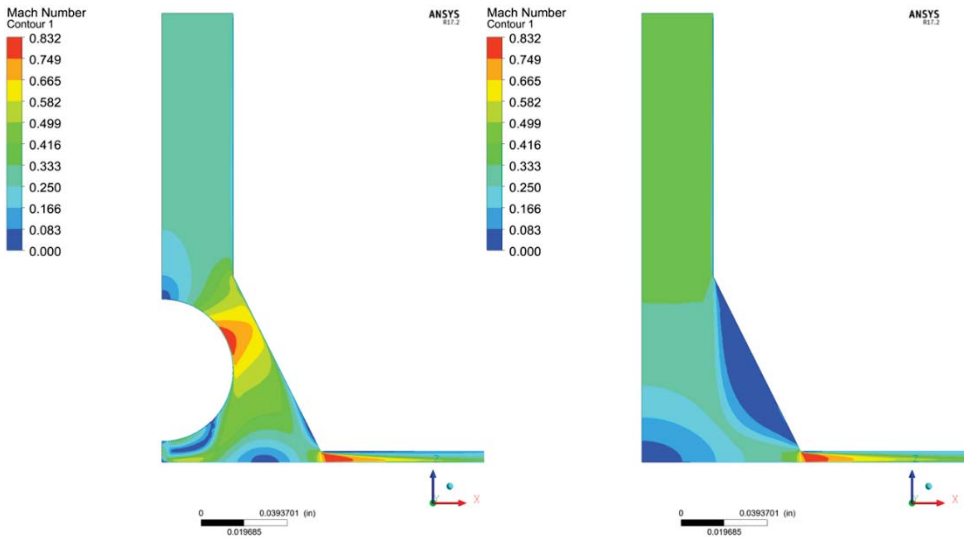

Figure 9: Comparison of Velocity Profiles in a Diffuser With and Without an Obstruction

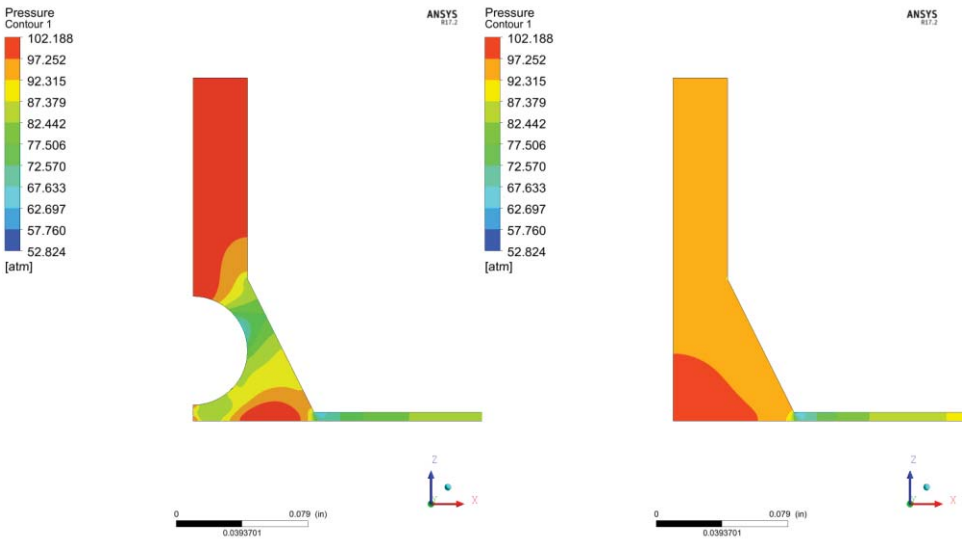

Figure 10: Pressure Distribution Comparison in a Diffuser With and Without an Obstruction

Once the basic configuration was defined, the 20 degree model was used to analyze a variety of geometric combinations of nozzle diameter, pocket size and depth, and diffuser diameter. The following findings came out of the analysis performed:

- The nozzle diffuser has no significant benefit to the hydrostatic bearing system.
- The pocket size has the greatest effect on maximizing the restoring force.
- Increasing pocket depth reduces flow velocity and avoids supersonic flow at high pressure ratios.
- The nozzle diameter has less than a primary effect on force but quadratically changes flow rate. The selected diameter should result in a pocket pressure that is the average of the inlet and exhaust pressures in the center of the bearings load range.
- Too small of a nozzle can cause phase change as the static pressure drops below the critical pressure line. High pressure differential and small nozzle diameter causes high dynamic pressure (high velocity flow), reducing static pressure, possibly enabling such a problem.

Full Bearing CFD – Stiffness and Total Leakage Analysis

Based on the results in the previous section, the following geometry was selected for the full bearing CFD analysis:

- Bearing diameter: 2.50 inches
- Bearing length: 1.50 inches
- Radial clearance: 0.002 inch
- Pocket size: 0.875 inch
- Number of pocket/nozzle sets: 6

The geometry was created in SolidWorks to represent a quarter of the bearing, split along the

XY and XZ planes of symmetry (Figure 11). The model was parametrized to allow for updates to shaft eccentricity and other dimensions. The mesh was setup to accommodate these dimensional changes. Three shaft eccentricities were meshed, representing 25%, 50%, and 75% eccentricity (where 0% represents a perfectly centered shaft). Each mesh was analyzed at rotational speeds of 30,000, 40,000, and 50,000 rpm.

The quarter mesh was reflected about the XZ plane to achieve a 360 degree half bearing to accommodate shaft rotation. A total pressure of 1600 psi (11 MPa) and a total temperature of 257°F (125°C) were applied at each nozzle inlet, while a static pressure of 1300 psi was applied at the discharge plenum exit. Surfaces where the boundary conditions were imposed are illustrated in Figure 12. In post-processing the results, the following variables were tracked:

- Forces on the shaft
- Mass Flow Rate
- Minimum domain pressure (to avoid phase change)
- Maximum domain Mach number (to avoid sonic flow)
- General pressures and temperatures at the flow boundaries

Results from the quarter model analysis yielded the following performance for a complete bearing:

- Restoring force: 310 lbf
- Stiffness: 310,100 lbf/inch
- Minimum static pressure in domain: 1247 psi (no phase change)
- Maximum Mach number in domain: 0.463
- Total Flow Rate: 0.42 lbm/s

Figure 11: Quarter Model CAD Model and Meshed Geometry
Model was broken up into 40 mesh bodies for structured meshing.

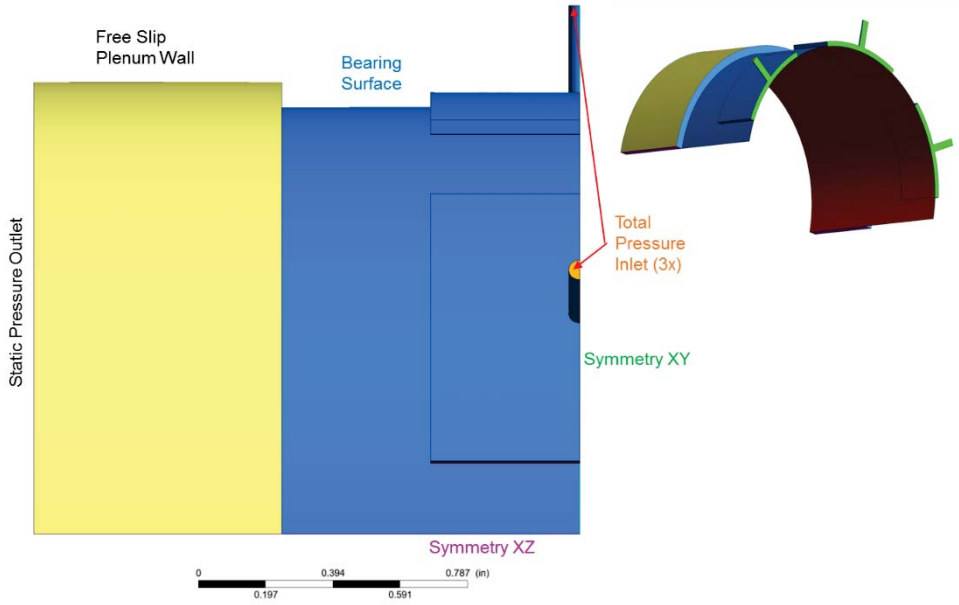

Figure 12: Illustration of Applied Boundary Conditions and Planes of Symmetry 1600 psi Total Pressure Inlet, 1300 psi Static Pressure Outlet

Contour plots showing the absolute pressure distribution and normalized pressure distribution in the quarter model run are shown in Figure 13 and Figure 14, respectively.

By introducing rotation to the model, the resultant load vector is no longer directly in line with the displacement. A tangential force, or cross-coupling force, is induced by the rotation, as illustrated in Figure 14. The rotation also has a significant effect on the total mass flow rate through the bearing. Figure 15 shows the influence shaft rotation has on the resulting force vector as well as mass flow rate through the bearing. Interestingly, the addition of rotation tends to reduce the mass flow through the bearing, which is an added benefit.

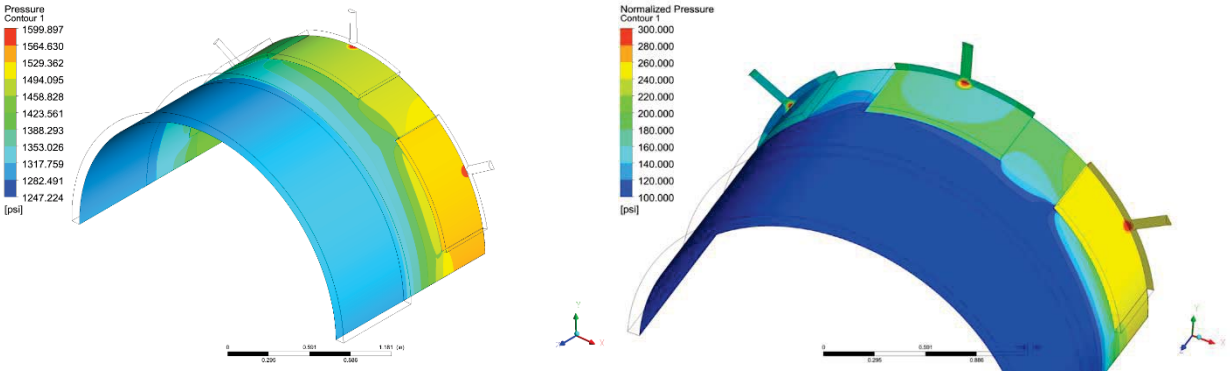

Figure 13: Absolute Pressure (left) and Normalized Pressure (right) Distributions in the Quarter Model (no Rotation) with 50% Eccentricity

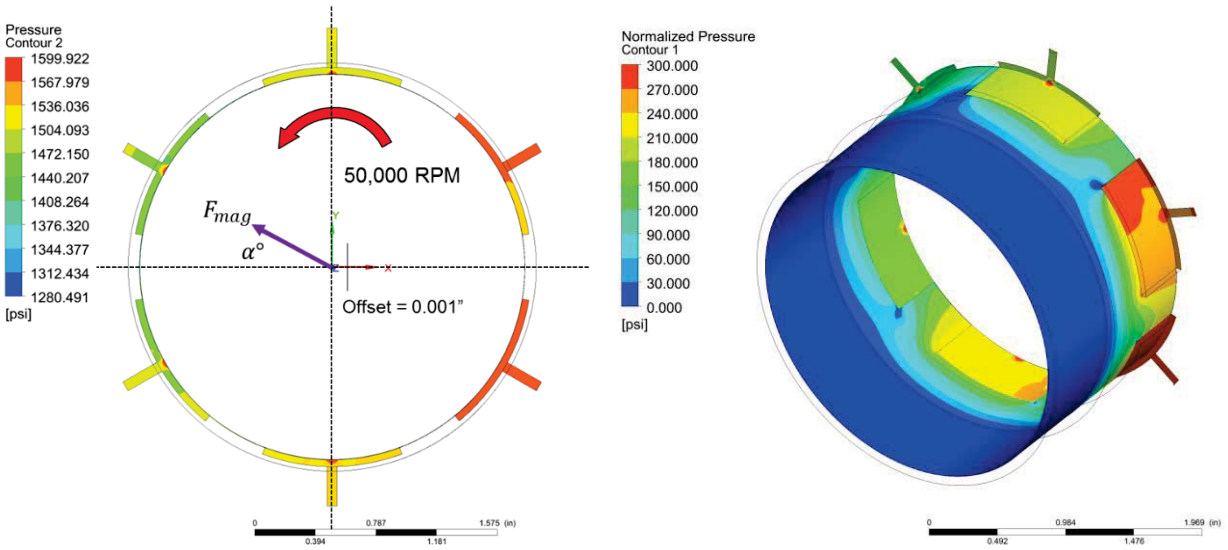

Figure 14: Absolute Pressure (left) and Normalized Pressure (right) Distributions in the Half Model at 50,000 rpm and 50% Eccentricity

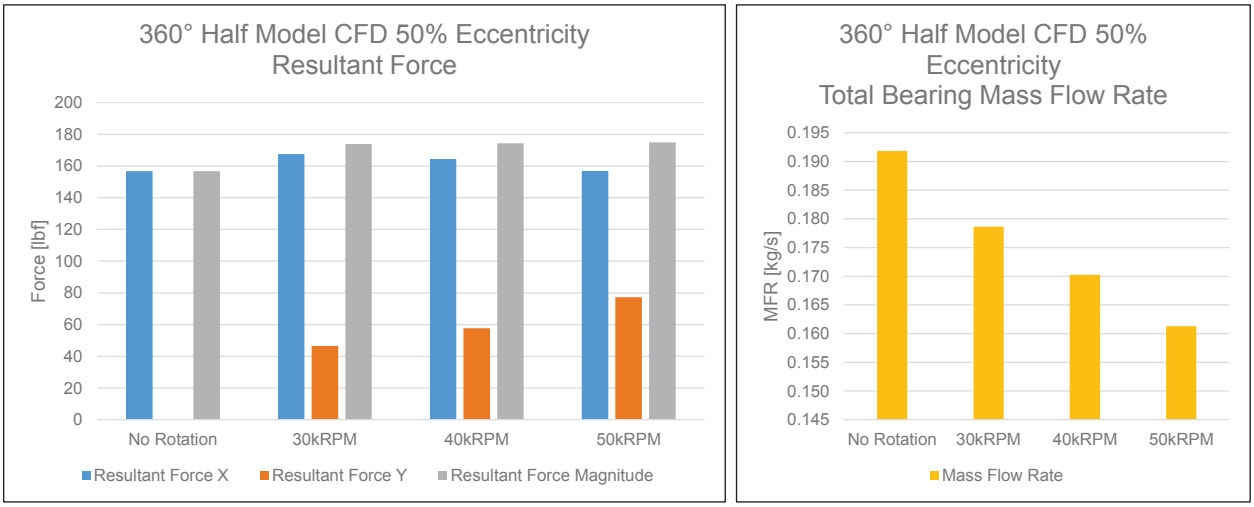

Figure 15: Influence of Rotational Speed on the Resultant Force Vector and Mass Flow Rate (X-axis is parallel to displacement, Y-axis is perpendicular to displacement)

Derivation of Stiffness and Damping Coefficients

Characterization of a bearing's stiffness and damping coefficients is critical if a bearing is to be implemented properly in a rotating machine's design. This was accomplish by using a modified frame of reference method following the spirit of Athavale and Hendricks[4] applied in a manner similar to Wagner[5] with reduced-order coefficient curve fits. Constant direct stiffness, direct damping, and cross-coupling coefficients were derived based on the assumption that rotor whirl would be in the range of 25% to 60% of the rotating speed. The technique, originally developed to derive the fluid stiffness and damping coefficients for axisymmetric seals, considers the transient problem of a rotor with a spinning frequency of ω rotating around the center of the stator (seal or bearing) with a whirling frequency of Ω and orbit radius e by

transferring it to a stationary problem using a rotating relative coordinate system as illustrated in Figure 16. This method allows for the derivation of constant radial and tangential forces on the shaft as the orbit is zero in the rotating relative coordinate system. Once the forces are derived from CFD, the stiffness, damping, and inertial coefficients can be calculated for a particular shaft eccentricity using second-order algebraic equations derived from three different whirl speeds. Resulting stiffness coefficients are plotted as a function of whirl ratio for 25 percent and 50 percent shaft eccentricities in Figure 17.

The applied technique is an attempt at simulating sub-synchronous whirl at fractions of operating speed. The bearing geometry is not axisymmetric and therefore the method is not exact, but it is cyclic-symmetric and therefore the author believes the approach is sufficiently representative of actual behavior. To validate the approach, the values obtained were compared against those estimated using Someya[6] and found that the calculated values of stiffness were within 10% of prediction, although the predicted damping coefficients were lower than Someya, and therefore conservative. On that basis the author proceeded with the design. Additionally, MSI is in the process of performing a full transient analysis of this design, as well as exploring a new algorithm developed by Remaki, et. al[7].

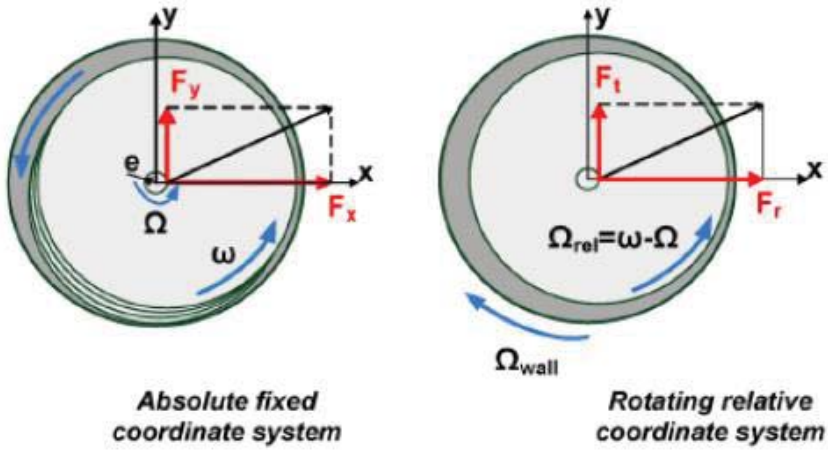

Figure 16: Illustration of CFD Coordinate Systems used in the Modified Frame of Reference Method

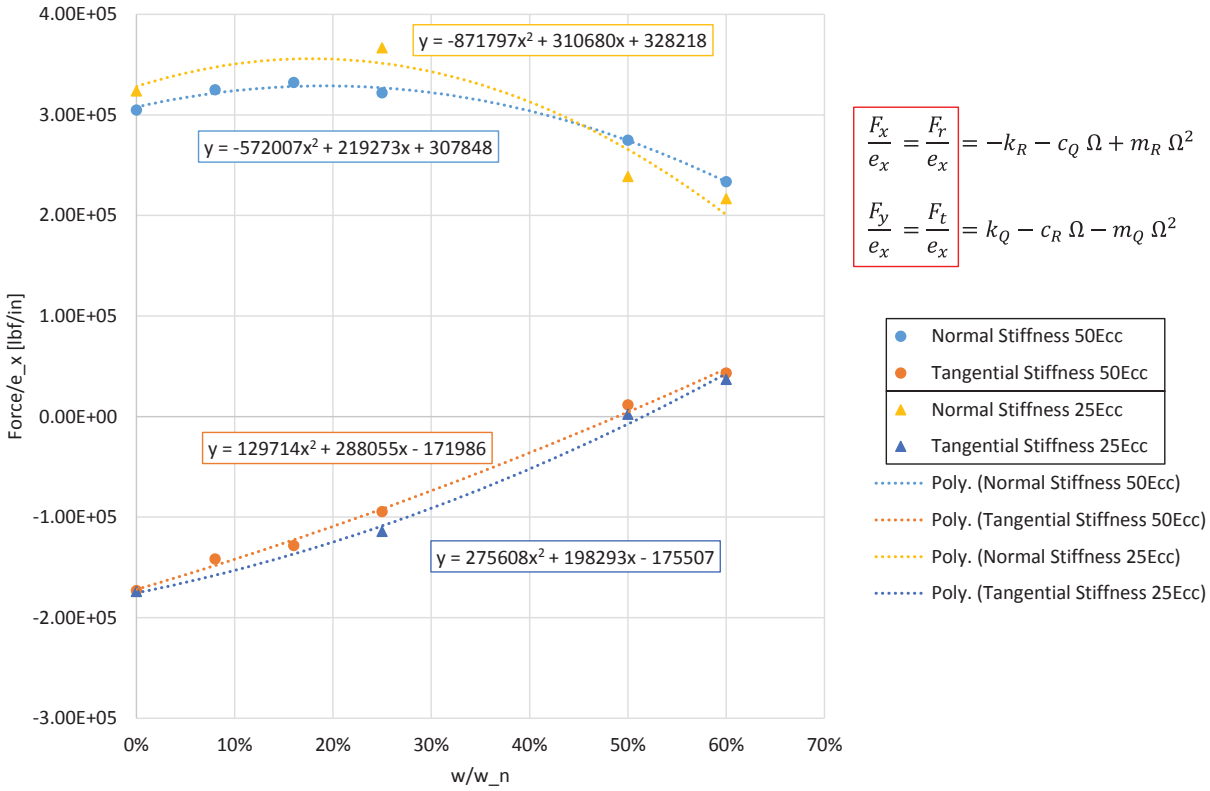

Figure 17: Normal and Tangential Stiffness Coefficients vs. Whirl Ratio for Shaft Eccentricities of 25 and 50 Percent

Radial Bearing Design Optimization – Groove Addition

In order to reduce the mass flow rate through the bearing, and minimize the impact on overall cycle efficiency, different geometry enhancements were investigated. The compliance of the foil itself helps to reduce pocket leakage versus that of a stiff bearing surface, while retaining good hydrostatic stiffness and load capacity. In addition to this, the most improvement was gained by adding grooves to the geometry. The grooves were aligned against the direction of rotation, thus effectively "pumping" some of the fluid back into the bearing, similar to a herringbone bearing design.

A sector model was selected due to geometry needs for meshing a semi-structured grid to capture near wall behavior within the grooves. The sector model consisted of a periodic geometry with a nominal radial film gap of 0.002 inch, as shown in Figure 18. Some optimization took place on the groove design, but mainly focused on groove depth. The normalized pressure profiles for the groove geometry with three different nozzle diameters is provided in Figure 19. A leakage reduction of over a factor of two was ultimately achieved by introducing the pumping groove design and re-optimizing the orifice size, without compromising the stiffness or load capacity of the bearing.

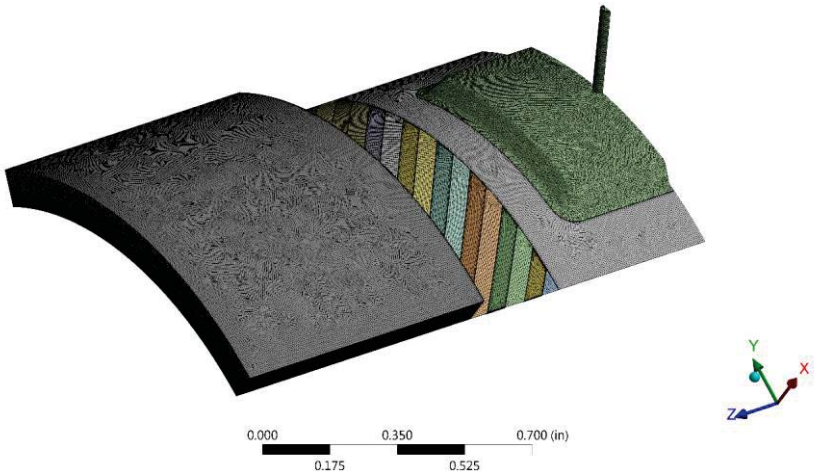

Figure 18: Sector Model Used to Evaluate Different Groove Geometries to Reduce Bearing Leakage

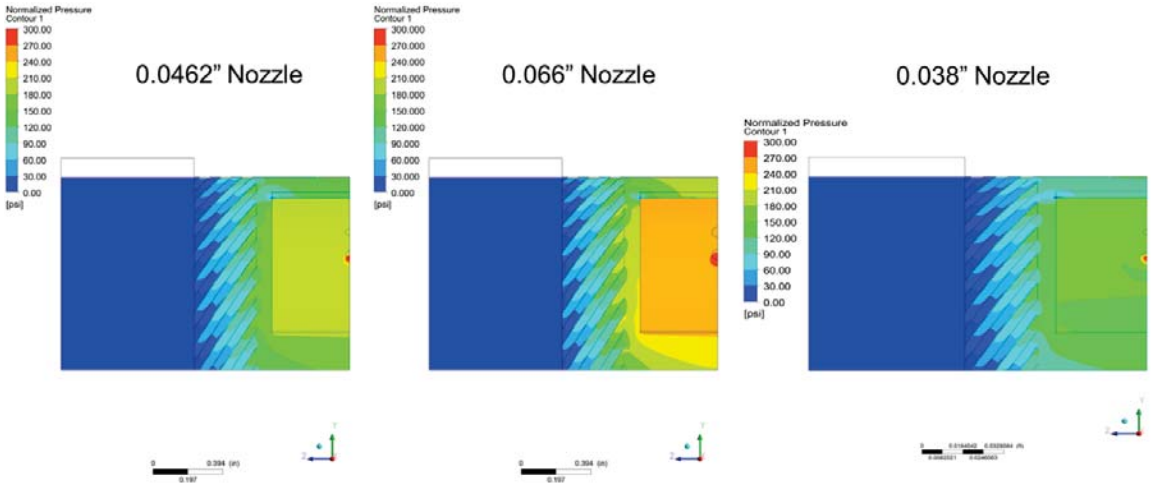

Figure 19: Normalized Pressure Distribution in a Grooved Bearing for Different Nozzle Diameters

Thrust Bearing Design & Analysis

A detailed analysis of the thrust bearing was also conducted. The double-acting thrust bearing was modeled as a 45 degree sector model with a nozzle/pocket on each side of the thrust disk (Figure 20). The thrust disk was offset by 0.001 inch within the total axial clearance of 0.004 inch. Total pressure on the nozzle inlets and static pressure on the radial outlet and two axial outlets on each side of the thrust disk established the control volume. Initially, different nozzle diameters were evaluated to maximize the restoring force on the thrust disk and minimize leakage flow. The normalized pressure distribution shown in Figure 21 illustrates the difference between the two sides with different axial clearances. Next, different groove designs were tested on the ID and OD of the thrust disk to reduce the leakage further, similar to that used in the radial bearing design.

Two different groove designs, log-spiral grooves and concentric radial grooves, were evaluated. The more complex log-spiral grooves showed only minor leakage reduction compared to the concentric radial grooves. It was believed that the log-spiral grooves would "pump" some of the fluid back into the pocket center more effectively, but due to centrifugal forces of an increasing radial flow path and the increased curtain leakage area created by the

groove passages, a significant reduction in leakage was not realized. The concentric radial grooves behaved as a labyrinth seal, increasing the pressure drop across the sealing lands and reducing the overall leakage rate. A simpler sector model was created for both the ID and OD ends of the thrust disk in order to optimize the grooved design. Features such as groove depth relative to film gap, number of grooves, and angle (log-spiral) were tested in the optimization study.

As a result of the study, a total of eight concentric grooves (four on the ID and four on the OD) on the thrust disk on both sides were determined to yield the lowest leakage rate. The study also showed that once flow interruption was achieved, further increase in the radial groove depth did not play a major role in leakage control.

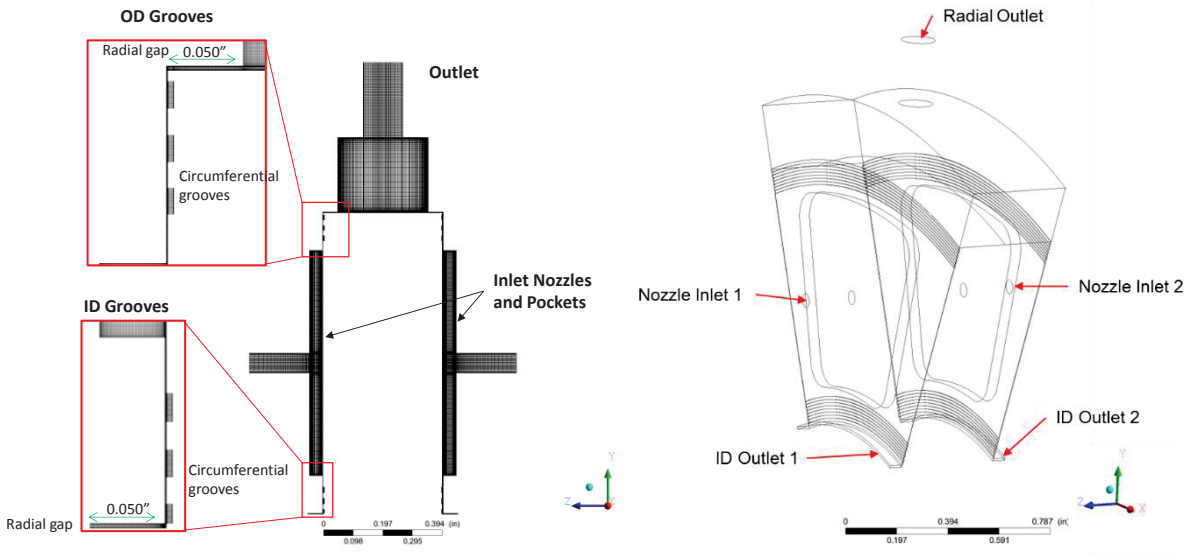

Figure 20: Double-Acting Thrust Bearing Sector Model Showing Concentric Groove Geometry

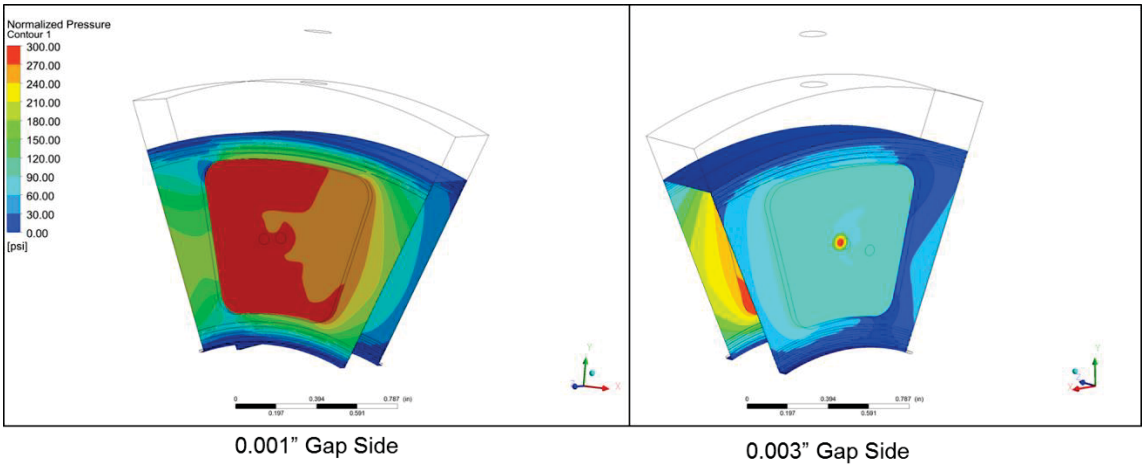

Figure 21: Normalized Pressure Distribution on Both Sides of the Thrust Disk

Final Thrust Bearing Design

Based on the results in the previous section, the following geometry was selected for the thrust bearing design:

- Outer diameter: 4.00 inches
- Inner diameter: 2.00 inches
- Axial clearance: 0.002 inch per side
- Pocket size: 0.875 inch
- Number of pocket/nozzle sets: 8
- 4 radially concentric grooves on the ID end and 4 grooves on the OD end.

This double-acting thrust bearing has the following performance characteristics:

- Total Axial Force for 0.001 inch deflection: 1286 lbf
- Total Flow Rate: 0.74 lbm/s
- Total Torque: 2.9908 lbf-ft

Ongoing and Future Work

Current efforts are focused on finalizing the detail designs of the bearings and generating manufacturing drawings. After completion of the detailed drawings, critical manufacturing processes will be identified and process specifications will be prepared. Components will be procured and inspected to ensure the drawing requirements are met. The bearings will then be assembled in MSI's foil bearing manufacturing facility. Critical dimensions and features of the finished bearings will be inspected and documented.

Test rig modifications will be completed as required to conduct the schedule of bearing tests. Tests will be conducted in both MSI's and Sandia National Laboratory's facilities. Parts will be procured for the test bearings and required test rig components. Controls and instrumentation requirements will be established, using existing in-house equipment to the extent possible. A full complement of testing will be conducted at both MSI's and Sandia's facilities, including validation testing in a sCO_2 environment. Data will be compiled and finally compared to the theoretical models. MSI personnel will be present at Sandia while testing is conducted. Testing is scheduled to be completed in June, 2018.

Summary

Based on the work conducted, the hybrid foil bearing designs show great promise for applications where sCO_2 is used as the working fluid. A similar bearing design should work well in other fluids as well. The characteristics of the sCO_2 fluid pose interesting challenges, both in performing the analysis as well as implementation in the design, but so far do not impose any absolute limitations. To date, MSI has analytically shown that the hydrostatic assist can generate enough load capacity to provide an effective sCO_2 turbomachine bearing design. It is anticipated that testing in sCO_2 will demonstrate foil bearing suitability in this very demanding environment.

REFERENCES

1. Chapman, P., “Advanced Gas Foil Bearing Design for Supercritical CO_2 Power Cycles,” Proceedings of the 5th International Symposium - Supercritical CO_2 Power Cycles, San Antonio, Texas, March 28-31, 2016.
2. Park, S., "Hybrid Air Foil Bearing with External Pressurization," A Thesis submitted to the Office of Graduate Studies of Texas A&M University, May 2007.
3. Kumar, M., "Analytical and Experimental Investigation of Hybrid Air Foil Bearings," A Thesis submitted to the Office of Graduate Studies of Texas A&M University, August 2008.
4. Athavale, M. M., and Hendricks, R. C., 1996, “A Small Perturbation CFD Method for Calculation of Seal Rotordynamic Coefficients,” Int. J. Rotating Mach., 2(3), pp. 167-177.
5. Wagner, N.G., Steff, K., Gausmann, R., Schmidt, M., “Investigations on the Dynamic Coefficients of Impeller Eye Labyrinth Seals,” Proceedings of the Thirty-eighth Turbomachinery Symposium, pp. 53-69, September 2009.
6. Someya, T., “Journal-Bearing Databook”, pp. 179-180, Springer-Verlag Berlin, 1989.
7. Remaki, L., Ramezani, A., Blanco, J., Garcia, I., “New Simplified Algorithm for the Multiple Rotating Frame Approach in Computational Fluid Dynamics,” ASME Journal of Fluids Engineering, Vol. 139, August, 2017.

ACKNOWLEDGEMENTS

This material is based upon work supported by the U.S. Department of Energy, Office of Science, Office of Fossil Energy, under Award Number DE-SC0013691.

DISCLAMER